Letter

Epidemic criticality in temporal networks

Chao-Ran Cai [1,2,*] Yuan-Yuan Nie,[1] and Petter Holme [3,4,†]
[1]School of Physics, Northwest University, Xi'an 710127, China
[2]Shaanxi Key Laboratory for Theoretical Physics Frontiers, Xi'an 710127, China
[3]Department of Computer Science, Aalto University, Espoo 02150, Finland
[4]Center for Computational Social Science, Kobe University, Kobe 657–8501, Japan

(Received 21 November 2023; accepted 21 February 2024; published 22 April 2024)

Analytical studies of network epidemiology almost exclusively focus on the extreme situations where the timescales of network dynamics are well separated (longer or shorter) from that of epidemic propagation. In realistic scenarios, however, these timescales could be similar, which has profound implications for epidemic modeling (e.g., one can no longer reduce the dimensionality of epidemic models). Combining Monte Carlo simulations and mean-field theory, we analyze the critical behavior of susceptible-infected-susceptible epidemics in the vicinity of the critical threshold on the activity-driven model of temporal networks. We find that the persistence of links in the network causes the threshold to decrease as the recovery rate increases. Dynamic correlations (coming from being close to infected nodes increases the likelihood of infection) drive the threshold in the opposite direction. These two counteracting effects make epidemic criticality in temporal networks a remarkably complex phenomenon.

DOI: 10.1103/PhysRevResearch.6.L022017

Introduction. The quest for epidemic models that are both realistic and analytically tractable is a fundamental challenge to theoretical research. This is never as difficult as when one cannot rely on ignoring a structure, by assuming it constant. When building an analytical theory, how fast the network changes and how fast the epidemic spreads are two dynamics that one would like to reduce to one. From a medical point of view, that might not work; an incipient outbreak might sweep over the population in a matter of weeks, the same timescale of updates to the friendship network [1,2]. This is the motivation for temporal network epidemiology, where the networks do not necessarily change slower or faster than the disease propagation [3–5].

There are three main philosophies of how to go beyond static network epidemiology to include the temporality of edges. The first approach treats temporal contacts as possible contagion events [6,7]. This approach often relies on empirical data of the contacts and analyzes them by computer simulations. The second approach, adaptive networks, models the contacts without real-world data but includes assumptions about how those contacts change given the state of the disease [8,9]. In this Letter, we will take a third approach, which is also purely model based, trying to emulate dynamic contact structures that real epidemics spread on while being tractable for analytical calculations. Typically, these models, such as blinking networks [10] and activity-driven networks [11,12], assume an underlying static network over which they generate active contacts.

The original activity-driven network model was proposed by Perra *et al.* [11], as follows. (i) The network is initialized to be completely disconnected and an activity $a_i = \eta x_i$ is assigned to each node i based on the given activity distribution $F(x)$. (ii) At each discrete time t, each node i becomes active with probability $a_i \Delta t$ and randomly creates m undirected links with other nodes. (iii) The epidemic dynamics take place over the instantaneous network. (iv) At the next time step $t + \Delta t$, all the links are removed and the process resumes from step (ii). The activity-driven network can be considered as the simplest yet nontrivial framework in which to study dynamical processes unfolding on temporal networks [13,14]. Only one variable $F(x)$ is time invariant and represents the degree distribution of an aggregated network [11–13,15,16]. Over the past decade, the epidemic dynamics on activity-driven networks have extended in different directions [17–31], including tackling real epidemiological models [21,29], the effects of heterogeneity [17,22,30], and the introduction of network features such as memory effects [19,24,25] and individual attractiveness distribution [23,31].

In static network epidemiology, the canonical models susceptible-infected-recovered and susceptible-infected-susceptible (SIS) are effectively governed by one parameter β/μ, the ratio of infection to recovery rate. Therefore, most studies of activity-driven networks also focused on this ratio [11,17,19,23,24,28–31]. This approach, effectively studying the model in the limit of fast network dynamics, goes against the idea of temporal networks as the modeling framework for intermediate timescales. In this limit, the β/μ-based

*ccr@nwu.edu.cn
†petter.holme@aalto.fi

mean-field approach accurately describes the criticality of compartmental models on activity-driven networks. However, reality can have slower network dynamics, and then the mean-field analysis will fail.

More precisely, the thresholds of both annealed (the limit of rapidly changing) and static (the limit of slowly changing) networks depend only on β/μ, but their actual critical values $(\beta/\mu)_c$ are different because of dynamical correlations in the static networks [32], i.e., infected nodes tend to group together. Since the activity-driven network can interpolate between these extremes, by keeping one of β or μ fixed, we can understand that tuning only the other must change the threshold (contradicting the assumption that β/μ fully describes the criticality of epidemics on the activity-driven model).

In this paper we employ a continuous-time description [20,33,34] of the coevolution of the network and SIS process. We use simulations to see the effects of both network correlations (reflecting the persistence of social contacts) and dynamic correlations caused by the inertia of the disease propagation. We complement these simulations with theoretical calculations that include the above-mentioned network correlations but ignore dynamic correlations. The comparison of these two types of results allows us to see the effects of the two types of correlations.

The rest of this paper is organized as follows. In Model we present a continuous-time description of the coevolution of temporal network and SIS dynamics. In Theoretical analysis for the SIS model on an activity- driven network we propose a theory that includes network correlations but ignores dynamic correlations to analyze epidemic threshold. In Results and discussion we present and analyze the main results of our model. In Conclusion we summarize our results.

Model. We turn to a technical definition of the model, a continuous-time description of the coevolution of the network and SIS dynamics. For the evolution of the network, each inactive (U) individual i is activated with a rate $a_i = \eta x_i$, where x_i is drawn from a probability distribution $F(x)$. When an individual gets activated, it randomly selects m individuals to generate links to. Active (A) individuals become unactivated with a rate b and then remove all links to themselves. Here the use of U instead of I for inactive individuals is to avoid confusion with the concept of the epidemic model. For the evolution of disease, we employ the classical SIS model. Susceptible (S) individuals become infected via contacts with infected (I) individuals at rate β times the number of susceptible-infected links. Infected individuals recover to susceptible with rate μ.

A continuous-time temporal network is a constantly changing network, similar to the evolution of dynamics, which does not remain the same for a long time and does not suddenly change drastically. The network is annealed when the network correlation is missing, while the network is approximately static for a large network correlation.

In this paper the simulation procedure is roughly divided into two steps. The activity-driven network is first evolved to equilibrium, corresponding to steps (i)–(iv). That means that the number of active individuals and the average degree of the network are stable. Then the initially infected individuals are randomly selected, corresponding to step (v). The network and dynamics coevolve to a dynamic equilibrium, that is, the number of infected individuals reaches a stable level, corresponding to steps (vi)–(viii). The detailed simulation procedure is as follows (see Supplemental Material [35] for a representative source code).

(i) Set $\tau = 0$, the network starts with N disconnected and inactive nodes.

(ii) At any time τ, we calculate each individual's transition rates $\lambda_i(\tau)$. The rate for any inactive individual becoming active is $\lambda_i(\tau) = a_i$. The rate for any active individual becoming inactive is $\lambda_i(\tau) = b$. Summing all of them yields the total transition rate $\omega(\tau) = \sum_i \lambda_i(\tau)$.

(iii) Time is incremented by $d\tau = 1/\omega(\tau)$. The individual whose state is chosen to change at time $\tau + d\tau$ is sampled with a probability proportional to $\lambda_i(\tau)$. The selected individual changes their state. When the selected individual is activated, they randomly select m individuals to generate links. When the selected individual becomes inactive, they delete all links to themself.

(iv) Repeat steps (ii) and (iii) until the number of active individuals and the average degree of the network are stable. The stability condition is set well above the convergence time as assessed by visual inspection for each parameter value. This approach is feasible since the activity-driven model does not have large fluctuations in the network structure between runs.

(v) Set $t = 0$; then $I_0 = N/100$ initially infected individuals are randomly selected.

(vi) At any time t, we calculate each individual's transition rates of the network state $\lambda_1^i(t)$ and those of the dynamic state $\lambda_2^i(t)$. The rate for any inactive individual becoming active is $\lambda_1^i(t) = a_i$. The rate for any active individual becoming inactive is $\lambda_1^i(t) = b$. The rate for any susceptible individual becoming infected is $\lambda_2^i(t) = \beta k_{\text{inf}}$, where k_{inf} is the number of infected neighbors of the focal individual. The rate for any infected individual recovering is $\lambda_2^i(t) = \mu$. Summing all of them yields the total transition rate $\omega(t) = \sum_i [\lambda_1^i(t) + \lambda_2^i(t)]$.

(vii) Time is incremented by $dt = 1/\omega(t)$. The individual whose state is chosen to change at time $t + dt$ is sampled with a probability proportional to $\lambda_1^i(t) + \lambda_2^i(t)$. For the selected individual, one of their network and dynamic states is changed, and the probability sampling is proportional to $\lambda_1^i(t)/[\lambda_1^i(t) + \lambda_2^i(t)]$ and $\lambda_2^i(t)/[\lambda_1^i(t) + \lambda_2^i(t)]$. When the network state of the selected individual changes, the rules for generating or disconnecting links are the same as those in step (iii).

(viii) Repeat steps (vi) and (vii) until the number of infected individuals is stable. For each set of parameter values we choose, by visual inspection, the number of thermalization steps to be at least three times longer than the typical time to reach equilibrium or ρ^I is effectively zero.

The gap between the Monte Carlo simulations, which naturally include network and dynamic correlations, and the mean-field theory given in the next section, which includes only network correlations, shows that the mean-field theory is not enough. However, we do so in order to study network correlations in theoretical isolation and to observe the effect of dynamic correlations in comparison with simulation and theoretical results.

Theoretical analysis for the SIS model on an activity-driven network. We start by analyzing the network evolution, which is independent of the SIS model. We define ρ^{A_a} as the fraction

of active individuals with activity rate a and $\rho^A = \int \rho^{A_a} da$ as the total fraction of active individuals. The dynamic equation of the fraction of active individuals of class a in the network can be written as

$$\frac{d\rho^{A_a}}{dt} = a(1-\rho^{A_a}) - b\rho^{A_a}. \tag{1}$$

The first term of Eq. (1) represents the spontaneous creation of active individuals, while the second term represents the spontaneous annihilation. When the evolution of the network reaches its steady state, i.e., $\frac{d\rho^{A_a}}{dt} = 0$, we have

$$\rho^{A_a} = \frac{a}{a+b}, \quad \rho^A = \left\langle \frac{a}{a+b} \right\rangle, \tag{2}$$

where $\langle \frac{a}{a+b} \rangle = \int \frac{\eta x F(x)}{\eta x + b} dx$. We define $\langle k_{A,a} \rangle$ as the average degrees of active individuals in class a. Considering that the links created per unit time in a steady-state network system should be equal to the disconnected ones, we have

$$\int maN(1-\rho^{A_a}) da = \int bN\rho^{A_a} \langle k_{A,a} \rangle da. \tag{3}$$

Combining Eqs. (2) and (3), we obtain

$$\langle k_A \rangle = \langle k_{A,a} \rangle = m, \tag{4}$$

where $\langle k_A \rangle$ is the average degrees of active individuals. Equation (4) also implies that the average degrees of inactive individuals in different classes are the same and the average degree of inactive individuals is represented by $\langle k_U \rangle$.

Similarly, the number of links between active and inactive individuals is stable when the system reaches its steady state. Since $\int aN(1-\rho^{A_a}) da$ individuals are activated per unit time, the number of new links to the inactive individuals is $m(1-\rho^A) \int aN(1-\rho^{A_a}) da$. On the one hand, links are disconnected when the active node of the link deactivates. On the other hand, when an inactive node in the link is activated, the class of the link changes. Therefore, the amount of link reduction between active and inactive individuals per unit time is $\langle k_U \rangle \int N(1-\rho^{A_a})(a+b) da$. Note that the number of links between active and inactive individuals is equal to $\langle k_U \rangle \int N(1-\rho^{A_a}) da$, because there are no links between inactive and inactive individuals. According to the relation $m(1-\rho^A) \int aN(1-\rho^{A_a}) da = \langle k_U \rangle \int N(1-\rho^{A_a})(a+b) da$, we have $\langle k_U \rangle = m\langle \frac{a}{a+b} \rangle (1 - \langle \frac{a}{a+b} \rangle)$. By the relation $\langle k \rangle = \langle k_A \rangle \rho^A + \langle k_U \rangle (1-\rho^A)$, the average degree of the network is

$$\langle k \rangle = m\left\langle \frac{a}{a+b} \right\rangle \left(1 + \left\langle \frac{b}{a+b} \right\rangle^2\right). \tag{5}$$

Next we consider the coevolution of networks and epidemics. Since individuals are infected through links, the evolution of the disease cannot be separated from the evolution of the network. The individuals are classified as XY, where $X \in \{U, A\}$ and $Y \in \{S, I\}$. We introduce the notation ρ^{XY_a} for the fraction of individuals with state XY and class a; $\phi^{XY_a, X'Y'_{a'}}$ is the probability that an individual with state XY and class a is connected to an individual with state $X'Y'$ and class a'. Note that $\phi^{US_a, US_{a'}}$, $\phi^{UI_a, UI_{a'}}$, and $\phi^{US_a, UI_{a'}}$ would be zero.

From the above, we can state the master equations as

$$\frac{d\rho^{UI_a}}{dt} = \beta \int \phi^{US_a, AI_{a'}} da' - (a+\mu)\rho^{UI_a} + b\rho^{AI_a}, \tag{6a}$$

$$\frac{d\rho^{AI_a}}{dt} = \beta \int (\phi^{AS_a, AI_{a'}} + \phi^{AS_a, UI_{a'}}) da' + a\rho^{UI_a} - (b+\mu)\rho^{AI_a}. \tag{6b}$$

The term $\beta \int \phi^{XS_a, X'I_{a'}} da'$ represents that susceptible individuals are infected by an infected individual at rate β. The term $\mu\rho^{XI_a}$ represents that infected individuals recover spontaneously at rate μ. The term $a\rho^{UY_a}$ represents that inactive individuals are activated at rate a. The term $b\rho^{AY_a}$ represents that individuals change from active to inactive at rate b. Since only active individuals can make connections and inactive individuals cannot, we can approximate $\phi^{XY_a, X'Y'_{a'}}$ in Eq. (6) in the form of ρ^{XY_a} using the mean-field ansatz, i.e.,

$$\phi^{AS_a, AI_{a'}} = 2\langle k_A \rangle \rho^{AS_a} \rho^{AI_{a'}}, \tag{7a}$$

$$\phi^{AS_a, UI_{a'}} = \langle k_A \rangle \rho^{AS_a} \rho^{UI_{a'}}, \tag{7b}$$

$$\phi^{US_a, AI_{a'}} = \langle k_A \rangle \rho^{US_a} \rho^{AI_{a'}}. \tag{7c}$$

Note that the approximation of Eq. (7) means that we ignore dynamic correlations. By inserting Eq. (7) into Eq. (6) and then integrating both sides of Eq. (6) with respect to a, we get

$$\frac{d\rho^{AI}}{dt} = \left(2\beta m\left\langle \frac{a}{a+b} \right\rangle - b - \mu\right)\rho^{AI} - 2\beta m(\rho^{AI})^2 + \left(\beta m\left\langle \frac{a}{a+b} \right\rangle + \langle a \rangle\right)\rho^{UI} - \beta m \rho^{UI}\rho^{AI}, \tag{8a}$$

$$\frac{d\rho^{UI}}{dt} = \left(\beta m\left\langle \frac{b}{a+b} \right\rangle + b\right)\rho^{AI} - (\langle a \rangle + \mu)\rho^{UI} - \beta m \rho^{UI}\rho^{AI}, \tag{8b}$$

where $\rho^{UI} = \int \rho^{UI_a} da$ and $\rho^{AI} = \int \rho^{AI_a} da$. See Appendix A for a detailed derivation.

Now we perform a linear stability analysis for Eq. (8) around the fixed point $\rho^{AI} = \rho^{UI} = 0$, and after ignoring the higher-order terms, the Jacobian matrix of Eq. (8) can be written as

$$J = \begin{pmatrix} 2\beta m\left\langle \frac{a}{a+b} \right\rangle - b - \mu & \beta m\left\langle \frac{a}{a+b} \right\rangle + \langle a \rangle \\ \beta m\left\langle \frac{b}{a+b} \right\rangle + b & -\langle a \rangle - \mu \end{pmatrix}. \tag{9}$$

When the largest eigenvalue of the Jacobian matrix is null, we can obtain the epidemic threshold

$$\left(\frac{\beta}{\mu}\right)_c = G(\sqrt{1+H} - 1), \tag{10a}$$

$$G = \frac{2\mu + \langle a \rangle + b + \frac{\langle a \rangle}{\langle \frac{a}{a+b} \rangle}}{2m\mu\left\langle \frac{b}{a+b} \right\rangle}, \tag{10b}$$

$$H = \frac{4\mu(\mu + b + \langle a \rangle)\left\langle \frac{b}{a+b} \right\rangle}{\left\langle \frac{a}{a+b} \right\rangle \left(2\mu + \langle a \rangle + b + \frac{\langle a \rangle}{\langle \frac{a}{a+b} \rangle}\right)^2}. \tag{10c}$$

When the probability distribution $F(x)$ satisfies the δ distribution, i.e., $F(x) = \delta(x - x_0)$, G and H in Eq. (10) can be simplified to $G = \frac{(\eta x_0 + b)(\mu + \eta x_0 + b)}{bm\mu}$ and $H = \frac{b\mu}{\eta x_0(\mu + \eta x_0 + b)}$. It is clear that the epidemic threshold of Eq. (10) is dependent

on μ on the activity-driven network, which is an important difference between annealed and static limits. Specifically, as $\mu \gg a$ and $\mu \gg b$, the activity-driven network degenerates into the static network and the threshold of Eq. (10) can be rewritten as $(\frac{\beta}{\mu})_c = \frac{1}{m\langle\frac{b}{a+b}\rangle}(\sqrt{1/\langle\frac{a}{a+b}\rangle} - 1)$. In addition, as $\mu \ll a$ and $\mu \ll b$, the activity-driven network will degenerate into the annealed network, for which the threshold of Eq. (10) approximates $(\frac{\beta}{\mu})_c = \frac{1}{m(\langle\frac{a}{a+b}\rangle + \frac{\langle a\rangle}{\langle a\rangle+b})}$ by using Taylor expansion.

Results and discussion. We focus on the effect of recovery rate μ on epidemic spreading. In this paper we test epidemic spreading processes on activity-driven networks with two different probability distributions $F(x)$: the δ distribution $F(x) = \delta(x - x_0)$, which means that the active rate is identical for all individuals, and the scale-free distribution $F(x) \propto x^{-\gamma}$. Unless explicitly stated, from now on we set $b = 1$. For the δ distribution, we set $x_0 = 0.1$. For the scale-free distribution, we set $\gamma = 2.1$ and $x \in [10^{-3}, 1]$.

A. Epidemic threshold and prevalence. Near the epidemic threshold, the order parameter fluctuates greatly, leading to a critical slowing. The latter means that the relaxation time of the order parameter tends to infinity in the thermodynamic limit. In general, the internal causes of divergence in relaxation time and divergence in thermodynamic susceptibility are the same. To estimate the threshold of SIS model on simulation, Ref. [36] proposed a method based on the relaxation time (on static networks) and Ref. [23] used this method on activity-driven networks. The relaxation time L is defined as the time that passes before the disease either goes extinct or spreads to a finite fraction C of the network (in our case $C = 0.25$), where C is the fraction of distinct nodes ever infected during the simulation. When β/μ is much less than its critical value $(\beta/\mu)_c$, the disease will quickly die out. If $\beta/\mu \gg (\beta/\mu)_c$, the disease rapidly reaches a steady state. For $\beta/\mu \sim (\beta/\mu)_c$, we can observe a longer relaxation time due to critical slowing down. In this case, the opposing mechanisms of infection and spontaneous recovery almost balance out, making spreading dynamics slow. In the thermodynamic limit, the average relaxation time diverges at $(\beta/\mu)_c$ both from below and from above. For finite systems, we use the maximum value of L to estimate the epidemic threshold.

The simulation results of Fig. 1 show an interesting nonmonotonic increase of the threshold with μ. Specifically, the curves show both local maxima and minima, whereas the analytical results are strictly decreasing. Meanwhile, the threshold tends to different saturation values in the static or the annealed limits. The simulation results will increase with the increase of μ when the analytical results tend to be saturated. It can be seen from the theoretical results that network correlation causes the threshold to decrease with the increase of μ, while the comparison between the theoretical and simulation results shows that dynamic correlations have the opposite effect.

We know that the average degree can regulate the strength of the dynamic correlations. In Fig. 2(a) we cause the threshold to monotonically increase with μ by significantly reducing the average degree (which means that the dynamic correlations are greatly enhanced). In contrast, Fig. 2(b) shows that the threshold decreases monotonically as μ increases, as the average degree increases substantially. In addition, we can see in Fig. 2(b) that the results from Eq. (10) match well with those obtained from Monte Carlo simulations.

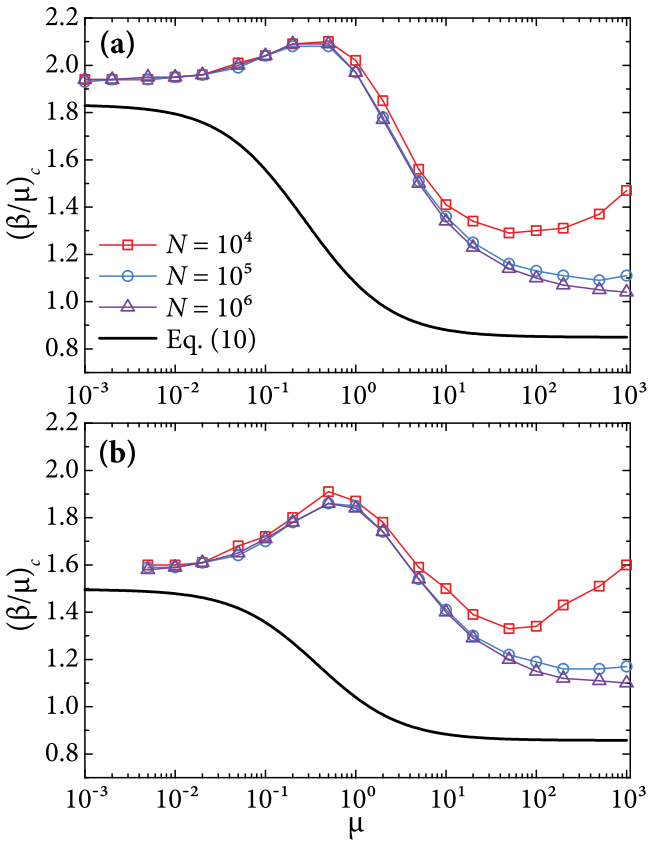

FIG. 1. Epidemic threshold as a function of recovery rate μ. The parameters are $m = 3$, $b = 1$, and (a) $\eta = 1$ and $F(x) = \delta(x - 0.1)$ and (b) $\eta = 28$ and $F(x) \propto x^{-2.1}$ with $x \in [10^{-3}, 1]$. The average degrees in (a) and (b) is approximately equal to 0.5 obtained by Eq. (5). Scatters are simulation results with an accuracy of 0.01. Lines are the theoretical estimations obtained from Eq. (10) that consider only the network correlations.

Next we plot the epidemic prevalence ρ^I as a function of β/μ for different μ in Fig. 3. The overall result is that the prevalence will gradually increase with the increase of β/μ, which is expected. For the analytic results in Fig. 3(b), we can see that ρ^I appears as a crossing behavior as a function of β/μ, which is a result of considering only the network correlation and ignoring the dynamic correlations. The crossing point occurs precisely at $\rho^I = 0.5$ and the corresponding $\beta/\mu = [m\langle a/(a+b)\rangle]^{-1}$, as detailed in Appendix B. For the simulation results of Fig. 3(a), we see that different curves no longer intersect precisely at one point, because the effects of dynamic correlations are not the same for different μ. Comparing the curves with high μ in Figs. 3(a) and 3(b), such as $\mu = 10$, we can see that ρ^I has a large drop for any β/μ, which means that dynamic correlations play a key role for high μ. In addition, we can see in Fig. 3 that our Eq. (8) can be used to predict the prevalence for low μ.

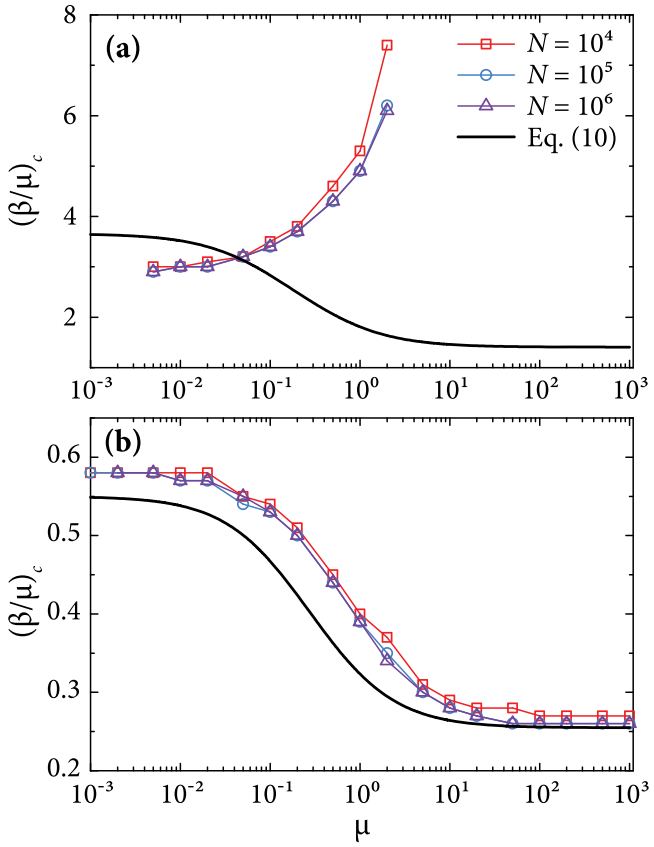

FIG. 2. Epidemic threshold as a function of recovery rate μ. The parameters are $b = 1$ and (a) $m = 3$, $\eta = 10$, and $F(x) \propto x^{-2.1}$ with $x \in [10^{-3}, 1]$ and (b) $m = 30$, $\eta = 1$, and $F(x) = \delta(x - 0.1)$. The average degrees are approximately equal to (a) 0.23 and (b) 1.66. The accuracy of simulation results is (a) 0.1 and (b) 0.01.

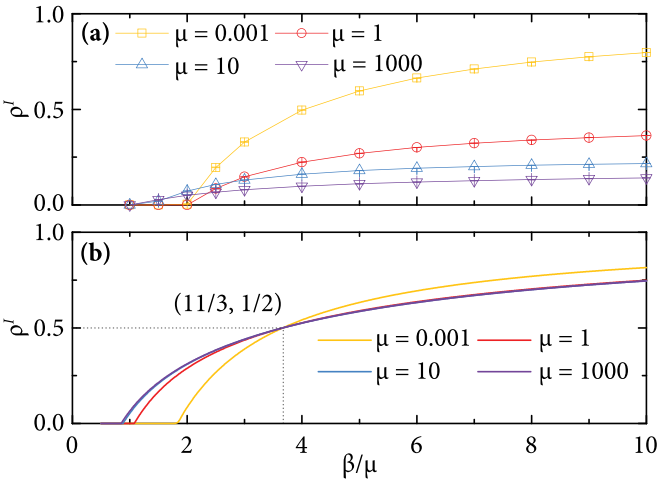

FIG. 3. Epidemic prevalence ρ^I as a function of β/μ for different recovery rate μ. The parameters are $N = 10^5$, $m = 3$, $\eta = 1$, $F(x) = \delta(x - 0.1)$, and $b = 1$. (a) The scatter plot shows simulation results from averages over 100 independent runs. (b) Lines are the theoretical estimations obtained from Eq. (8).

B. Average degree of the temporal network. In Fig. 4 we plot the time series of the fraction of active individuals, the average degree of active individuals, and the average degree of the network. The simulation results, which are denoted by light gray lines, are ten independent realizations. The analytical solutions of ρ^A, $\langle k_A \rangle$, and $\langle k \rangle$ are denoted by the red, blue, and purple lines, respectively. It is obvious from Fig. 4 that there is excellent agreement between the analytical solutions and the simulation results. Since we consider theoretically the correlation of network evolution, this allows the fraction of the average degree of active individuals to be accurately predicted, which provides the basic guarantee for the discussion in Epidemic threshold and prevalence.

Conclusion. We have investigated the effects of network correlation and dynamic correlations on SIS epidemics of activity-driven networks. In particular, we analyzed the effect of network correlation in isolation by mean-field theory, as well as the effect of dynamic correlations by comparing theoretical and simulation results. As the recovery rate μ increases, the threshold $(\beta/\mu)_c$ decreases for the effect of network correlation but increases for the effect of dynamic correlations. Because of this competitive relationship, the curves of the threshold show three types of behavior, which are monotonically increasing, monotonically decreasing, and first increasing and then decreasing but increasing again. Meanwhile, the effect of network correlation means that the prevalence produces a crossing behavior and the effect of dynamic correlations substantially reduces the prevalence. Finally, our theory can predict the threshold when the average degree $\langle k \rangle$ is high and predict the prevalence for fast recovery compared to network dynamics.

As a final remark, we hope our study will provide an opportunity for other analytical studies of the full two-dimensional parameter space of the SIS model on temporal networks. For example, it is always bimodal for the instantaneous degree distribution of the current activity-driven network, and it is not clear whether other network structures will exhibit completely different properties. Specifically, we can change the instantaneous degree distribution by changing the parameter m from a fixed value to a corresponding function. Meanwhile, we can consider applying our ideas to broader dynamics on temporal networks, such as synchronization dynamics [37–39] and directed percolation [40,41].

Acknowledgments. This work was supported by the Shaanxi Fundamental Science Research Project for Mathematics and Physics (Grant No. 22JSQ003). P.H. was supported by Japan Society for the Promotion of Science Grant No. JP 21H04595.

Appendix A: Derivation of Eq. (8). By inserting Eq. (7) into Eq. (6) we have

$$\frac{d\rho^{UI_a}}{dt} = \beta m \int \rho^{US_a} \rho^{AI_{a'}} da' - (a + \mu)\rho^{UI_a} + b\rho^{AI_a},$$
$$\frac{d\rho^{AI_a}}{dt} = \beta m \int (2\rho^{AS_a} \rho^{AI_{a'}} + \rho^{AS_a} \rho^{UI_{a'}}) da' + a\rho^{UI_a} - (b + \mu)\rho^{AI_a}. \quad \text{(A1)}$$

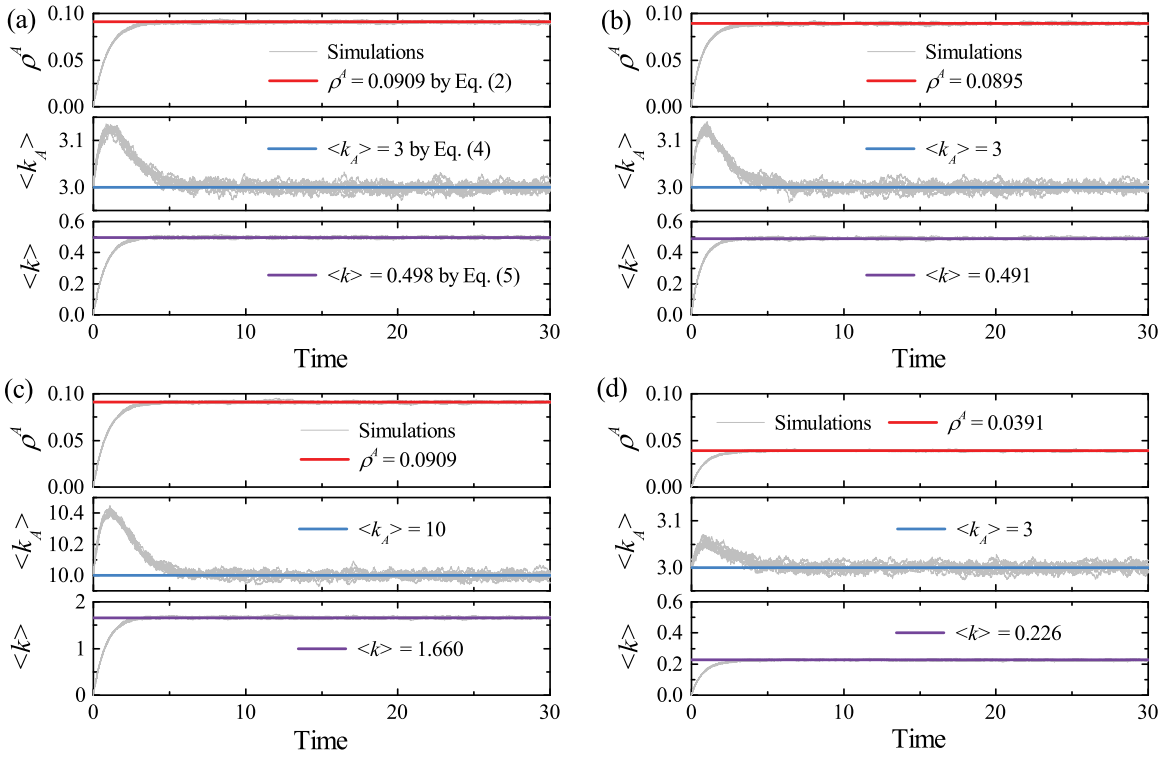

FIG. 4. Time series for the fraction of active individuals, the average degree of active individuals, and the average degree of the whole network. The light gray lines are simulation results of ten independent runs. The thick red, blue, and purple lines are obtained from Eqs. (2), (4), and (5), respectively. The parameters are $N = 10^5$, $b = 1$, and (a) $m = 3$, $\eta = 1$, and $F(x) = \delta(x - 0.1)$; (b) $m = 3$, $\eta = 28$, and $F(x) \propto x^{-2.1}$ with $x \in [10^{-3}, 1]$; (c) $m = 10$, $\eta = 1$, and $F(x) = \delta(x - 0.1)$; and (d) $m = 3$, $\eta = 10$, and $F(x) \propto x^{-2.1}$ with $x \in [10^{-3}, 1]$.

Combining with $\rho^{US_a} = 1 - \rho^{A_a} - \rho^{UI_a}$, $\rho^{AS_a} = \rho^{A_a} - \rho^{AI_a}$, and Eq. (2), Eq. (A1) is written as

$$\begin{aligned}\frac{d\rho^{UI_a}}{dt} &= \beta m\left(\frac{b}{a+b} - \rho^{UI_a}\right)\int \rho^{AI_{a'}}da' - (a+\mu)\rho^{UI_a} \\ &\quad + b\rho^{AI_a}, \\ \frac{d\rho^{AI_a}}{dt} &= \beta m\left(\frac{a}{a+b} - \rho^{AI_a}\right)\int (2\rho^{AI_{a'}} + \rho^{UI_{a'}})da' \\ &\quad + a\rho^{UI_a} - (b+\mu)\rho^{AI_a}. \end{aligned} \tag{A2}$$

We define ρ^{UI} and ρ^{AI} as the fractions of individuals in the inactive-infected state and the active-infected state, respectively, i.e., $\rho^{UI} = \int \rho^{UI_a}da$ and $\rho^{AI} = \int \rho^{AI_a}da$. By integrating both sides of Eq. (A2) with respect to a we get

$$\begin{aligned}\frac{d\rho^{UI}}{dt} &= \beta m\left\langle\frac{b}{a+b}\right\rangle\rho^{AI} - \beta m\rho^{UI}\rho^{AI} - \int a\rho^{UI_a}da \\ &\quad + \mu\rho^{UI} + b\rho^{AI}, \\ \frac{d\rho^{AI}}{dt} &= \beta m\left(\left\langle\frac{a}{a+b}\right\rangle - \rho^{AI}\right)(2\rho^{AI} + \rho^{UI}) \\ &\quad + \int a\rho^{UI_a}da - (b+\mu)\rho^{AI}. \end{aligned} \tag{A3}$$

According to Eqs. (4) and (5), we know that the degree distribution of any class a is the same bimodal distribution. Since we have ignored dynamic correlations [see Eq. (7)], ρ^{UI_a} in steady state is independent of a, that is,

$$\rho^{UI} = \rho^{UI_a}. \tag{A4}$$

Finally, by inserting Eq. (A4) into Eq. (A3), we can obtain Eq. (8).

Appendix B: Theoretical Solution for the Special Prevalence $\rho^I = 0.5$. We define ρ^{I_a} (ρ^{S_a}) as the fraction of individuals in the infected (susceptible) state and class a. According to Eq. (A1), we have

$$\frac{d\rho^{I_a}}{dt} = -\mu\rho^{I_a} + \beta m\int(\rho^{S_a}\rho^{AI_{a'}} + \rho^{AS_a}\rho^{I_{a'}})da'. \tag{B1}$$

We define ρ^I and ρ^S as the numbers of individuals in the infected state and in the susceptible state, respectively, i.e., $\rho^I = \int \rho^{I_a}da$ and $\rho^S = \int \rho^{S_a}da$. By integrating both sides of Eq. (B1) with respect to a we get

$$\frac{d\rho^I}{dt} = -\mu\rho^I + \beta m(\rho^S\rho^{AI} + \rho^{AS}\rho^I). \tag{B2}$$

Considering the special steady state $\rho^I = \rho^S = 0.5$, we have

$$\frac{\beta}{\mu} = \frac{1}{m\rho^A} = \frac{1}{m\left\langle\frac{a}{a+b}\right\rangle}. \tag{B3}$$

[1] N. H. Fefferman and K. L. Ng, How disease models in static networks can fail to approximate disease in dynamic networks, Phys. Rev. E **76**, 031919 (2007).

[2] S. Bansal, J. Read, B. Pourbohloul, and L. A. Meyers, The dynamic nature of contact networks in infectious disease epidemiology, J. Biol. Dyn. **4**, 478 (2010).

[3] N. Masuda and P. Holme, Predicting and controlling infectious disease epidemics using temporal networks, F1000Prime Rep. **5**, 6 (2013).

[4] N. Masuda and P. Holme, Introduction to temporal network epidemiology, in *Temporal Network Epidemiology* (Springer, Singapore, 2017), pp. 1–16.

[5] D. Soriano-Paños, G. Ghoshal, A. Arenas, and J. Gómez-Gardeñes, Impact of temporal scales and recurrent mobility patterns on the unfolding of epidemics, J. Stat. Mech. (2020) 024006.

[6] P. Holme, Temporal network structures controlling disease spreading, Phys. Rev. E **94**, 022305 (2016).

[7] P. de Castro, F. Urbina, A. Norambuena, and F. Guzmán-Lastra, Sequential epidemic-like spread between agglomerates of self-propelled agents in one dimension, Phys. Rev. E **108**, 044104 (2023).

[8] T. Gross, C. J. D. D'Lima, and B. Blasius, Epidemic dynamics on an adaptive network, Phys. Rev. Lett. **96**, 208701 (2006).

[9] P. C. Ventura, A. Aleta, F. A. Rodrigues, and Y. Moreno, Epidemic spreading in populations of mobile agents with adaptive behavioral response, Chaos Soliton. Fract. **156**, 111849 (2022).

[10] M. Hasler, V. Belykh, and I. Belykh, Dynamics of stochastically blinking systems. Part I: Finite time properties, SIAM J. Appl. Dyn. Syst. **12**, 1007 (2013).

[11] N. Perra, B. Gonçalves, R. Pastor-Satorras, and A. Vespignani, Activity driven modeling of time varying networks, Sci. Rep. **2**, 469 (2012).

[12] S. Liu, N. Perra, M. Karsai, and A. Vespignani, Controlling contagion processes in activity driven networks, Phys. Rev. Lett. **112**, 118702 (2014).

[13] B. Ribeiro, N. Perra, and A. Baronchelli, Quantifying the effect of temporal resolution on time-varying networks, Sci. Rep. **3**, 3006 (2013).

[14] A. Moinet, M. Starnini, and R. Pastor-Satorras, Random walks in non-Poissoinan activity driven temporal networks, New J. Phys. **21**, 093032 (2019).

[15] M. Starnini and R. Pastor-Satorras, Topological properties of a time-integrated activity-driven network, Phys. Rev. E **87**, 062807 (2013).

[16] M. Karsai, N. Perra, and A. Vespignani, Time varying networks and the weakness of strong ties, Sci. Rep. **4**, 4001 (2014).

[17] A. Rizzo, M. Frasca, and M. Porfiri, Effect of individual behavior on epidemic spreading in activity-driven networks, Phys. Rev. E **90**, 042801 (2014).

[18] E. Valdano, L. Ferreri, C. Poletto, and V. Colizza, Analytical computation of the epidemic threshold on temporal networks, Phys. Rev. X **5**, 021005 (2015).

[19] K. Sun, A. Baronchelli, and N. Perra, Contrasting effects of strong ties on SIR and SIS processes in temporal networks, Eur. Phys. J. B **88**, 326 (2015).

[20] L. Zino, A. Rizzo, and M. Porfiri, Continuous-time discrete-distribution theory for activity-driven networks, Phys. Rev. Lett. **117**, 228302 (2016).

[21] A. Rizzo, B. Pedalino, and M. Porfiri, A network model for Ebola spreading, J. Theor. Biol. **394**, 212 (2016).

[22] E. Ubaldi, N. Perra, M. Karsai, A. Vezzani, R. Burioni, and A. Vespignani, Asymptotic theory of time-varying social networks with heterogeneous activity and tie allocation, Sci. Rep. **6**, 35724 (2016).

[23] I. Pozzana, K. Sun, and N. Perra, Epidemic spreading on activity-driven networks with attractiveness, Phys. Rev. E **96**, 042310 (2017).

[24] M. Tizzani, S. Lenti, E. Ubaldi, A. Vezzani, C. Castellano, and R. Burioni, Epidemic spreading and aging in temporal networks with memory, Phys. Rev. E **98**, 062315 (2018).

[25] L. Zino, A. Rizzo, and M. Porfiri, Modeling memory effects in activity-driven networks, SIAM J. Appl. Dyn. Syst. **17**, 2830 (2018).

[26] P. Hu, L. Ding, and X. An, Epidemic spreading with awareness diffusion on activity-driven networks, Phys. Rev. E **98**, 062322 (2018).

[27] A. Moinet, R. Pastor-Satorras, and A. Barrat, Effect of risk perception on epidemic spreading in temporal networks, Phys. Rev. E **97**, 012313 (2018).

[28] M. Nadini, A. Rizzo, and M. Porfiri, Epidemic spreading in temporal and adaptive networks with static backbone, IEEE Trans. Netw. Sci. Eng. **7**, 549 (2020).

[29] F. Parino, L. Zino, M. Porfiri, and A. Rizzo, Modelling and predicting the effect of social distancing and travel restrictions on COVID-19 spreading, J. R. Soc. Interface **18**, 20200875 (2021).

[30] N. Gozzi, M. Scudeler, D. Paolotti, A. Baronchelli, and N. Perra, Self-initiated behavioral change and disease resurgence on activity-driven networks, Phys. Rev. E **104**, 014307 (2021).

[31] B. Wang, Z. Xie, and Y. Han, Impact of individual behavioral changes on epidemic spreading in time-varying networks, Phys. Rev. E **104**, 044307 (2021).

[32] C.-R. Cai, Z.-X. Wu, M. Z. Q. Chen, P. Holme, and J.-Y. Guan, Solving the dynamic correlation problem of the susceptible-infected-susceptible model on networks, Phys. Rev. Lett. **116**, 258301 (2016).

[33] K. Y. Leung and O. Diekmann, Dangerous connections: On binding site models of infectious disease dynamics, J. Math. Biol. **74**, 619 (2017).

[34] J. P. Rodríguez, M. Paoluzzi, D. Levis, and M. Starnini, Epidemic processes on self-propelled particles: Continuum and agent-based modeling, Phys. Rev. Res. **4**, 043160 (2022).

[35] See Supplemental Material at http://link.aps.org/supplemental/10.1103/PhysRevResearch.6.L022017 for a representative code.

[36] M. Boguñá, C. Castellano, and R. Pastor-Satorras, Nature of the epidemic threshold for the susceptible-infected-susceptible dynamics in networks, Phys. Rev. Lett. **111**, 068701 (2013).

[37] S. N. Chowdhury, S. Majhi, M. Ozer, D. Ghosh, and M. Perc, Synchronization to extreme events in moving agents, New J. Phys. **21**, 073048 (2019).

[38] S. N. Chowdhury, S. Majhi, and D. Ghosh, Distance dependent competitive interactions in a frustrated network of mobile agents, IEEE Trans. Netw. Sci. Eng. **7**, 3159 (2020).

[39] G. Mikaberidze, S. N. Chowdhury, A. Hastings, and R. M. D'Souza, Consensus formation among mobile agents in networks of heterogeneous interaction venues, Chaos Soliton. Fract. **178**, 114298 (2024).

[40] A. Badie-Modiri, A. K. Rizi, M. Karsai, and M. Kivelä, Directed percolation in temporal networks, Phys. Rev. Res. **4**, L022047 (2022).

[41] A. Badie-Modiri, A. K. Rizi, M. Karsai, and M. Kivelä, Directed percolation in random temporal network models with heterogeneities, Phys. Rev. E **105**, 054313 (2022).